

Study of the Optoelectronic Properties of Ultraviolet Photodetectors Based on Zn-Doped CuGaO₂ Nanoplate/ZnO Nanowire Heterojunctions

Xiaoyi Wang, Hongda Wu, Guanxin Wang, Xiaohui Ma,* Yingtian Xu,* He Zhang, Liang Jin, Linlin Shi, Yonggang Zou, Jingzhi Yin, and Dongxu Zhao

This study reports ultraviolet (UV) photodetectors based on CuGaO₂ (CGO) nanoplates (NPs) and Zn-doped CGO (CZGO) NP/ZnO nanowire (NW) heterojunctions. The vertical arrays of ZnO NWs are uniformly grown on the surface of hexagonal CZGO NPs and form a high-density p–n junction. The heterojunctions have better optoelectronic performance parameters than pure CGO NPs. Especially, the responsivity value of CZGO NP/ZnO NW heterojunctions reaches 0.12 A W⁻¹, and the photo-to-current ratio is estimated to be 4.5. This work offers a new idea for the rational design of optoelectronic devices from the synergistic effect of p-type CZGO NPs and n-type nanostructures.

1. Introduction

Photodetectors (PDs) convert optical radiation into electrical signals by the photoelectric effect.^[1,2] Through the gradual exploration of PDs, it has been proved that PDs can be applied to many fields,^[3] such as chemical monitoring,^[4] environment,^[5] biological analysis,^[6,7] future memory,^[8] and civil and military applications.^[9–12] Due to high sensitivity and fast time response, ultraviolet (UV) PDs have attracted wide attention.^[13] Wide-bandgap semiconductor materials commonly used in the UV PDs include diamond,^[14] ZnO,^[15] TiO₂,^[16] SnO₂,^[17] and ZnS.^[18] However, the ultrawide bandgap (5.5 eV) of diamond material is sensitive to deep UV light (wavelength less than 225 nm),^[19]

which results in poor detection performance of diamond-based devices. The high recombination rate and surface defects of photogenerated electron–hole pairs in wide-bandgap semiconductor materials seriously affect the efficiency of photoresponse. Therefore, the low quality of materials has become an important problem currently restricting the development of wide-bandgap semiconductors. Meanwhile, the use of low-dimensional wide-bandgap inorganic semiconductor nanostructure materials for building UV PDs has attracted intense attention.^[20]

The fabrication of detectors needs to keep pace with the development of modern electronic systems: energy saving, portability, and miniaturization.^[21,22] It is necessary to find a simple method to synthesize wide-bandgap materials with low-dimensional materials and improve the properties of materials by doping or constructing heterojunctions.

The p-type delafossite material ABO₂ (B = Cr, Al, Ga) generally relies on hole conduction.^[23] It is a new metal oxide with a bandgap greater than the upper limit of visible photon energy (3.11 eV). Considering that substituting trivalent cations by divalent cations in the structure effectively improves the p-type conductivity and carrier concentration of delafossite materials, they hold great attraction as p-type materials in UV optoelectronic devices.^[24] In recent years, researchers have proved that the calculated indirect bandgap width of CuGaO₂ (CGO) NPs is ≈1.9 eV; the direct allowed transition on one side of the broad bandgap is calculated as 3.5 eV.^[25] Therefore, CGO could be classified as a wide-bandgap semiconductor material. CGO is an intrinsic p-type material and one of the delafossite family, with excellent hole mobility.^[26] In contrast to CGO, n-type zinc oxide (ZnO) has a wide direct bandgap (3.37 eV) and large exciton binding energy (60 meV) at room temperature.^[27–29] In the UV optical detection system,^[30] when 1D ZnO nanowires (NWs) were combined with other low-dimensional materials such as metals, semiconductor nanoparticles, and 1D nanotubes and 2D materials,^[31] the increase of the specific surface area improves the detection performance. Considering the high matching lattice parameters between ZnO and CGO (the lattice mismatch is ≈10%), it is feasible to form a heterogeneous relationship at the interface. In addition, p-type CGO nanoplates (NPs) and n-type ZnO NWs can form a II-type staggered band arrangement that promotes the transfer of excitation holes and electrons.^[32] CGO NPs were synthesized by a

X. Wang, H. Wu, G. Wang, Prof. X. Ma, Prof. Y. Xu, Dr. H. Zhang, Dr. L. Jin, L. Shi, Prof. Y. Zou
State Key Laboratory of High Power Semiconductor Laser
Changchun University of Science and Technology
7186 Wei-Xing Road, Changchun 130022, P. R. China
E-mail: mxh@cust.edu.cn; xyt@cust.edu.cn

J. Yin
State Key Laboratory on Integrated Optoelectronics
College of Electronic Science and Engineering
Jilin University
2699 Qian-Jin Street, Changchun 130012, P. R. China

D. Zhao
State Key Laboratory of Luminescence and Applications
Changchun Institute of Optics, Fine Mechanics and Physics
Chinese Academy of Sciences
3888 Dongnanhu Road, Changchun 130021, P. R. China

 The ORCID identification number(s) for the author(s) of this article can be found under <https://doi.org/10.1002/pssb.201900684>.

DOI: 10.1002/pssb.201900684

hydrothermal method and crystallized into 2D hexagonal NPs of micron size due to the oriented attachment mechanism.^[33] Furthermore, the hole carrier concentration of CGO NPs can be improved by doping bivalent cations of Zn^{2+} and Mg^{2+} .^[34,35] In the CuGaO_2 phase, the ionic radius of Ga^{3+} is 0.062 nm,^[36] the ionic radius of Zn^{2+} is 0.074 nm,^[37] and the corresponding mismatch of ionic radii caused by the substitution of Ga^{3+} with Zn^{2+} is 19.3%. Tsay et al.^[38] have reported that the electrical properties of Zn-doped CuGaO_2 thin films are greater than those of Mg-doped CuGaO_2 thin films. This phenomenon was explained by the fact that the Zn-doped thin films had a smaller amount of the secondary phase than the Mg-doped thin films. Therefore, we chose Zn to dope CGO NPs, which inspired us to prepare Zn-doped CGO NPs and ZnO NW heterojunctions. This study reports the optoelectronic properties of UV PDs based on pure CGO NPs and Zn-doped CGO (CZGO) NP/ZnO NW heterojunctions. The morphology and composition of pure CGO NPs and CZGO NP/ZnO NW heterojunctions were characterized by scanning electron microscopy (SEM), X-ray diffraction (XRD), and X-ray photoelectron spectroscopy (XPS). The heterojunctions were found to have large specific surface area and photon capture ability. The responsiveness and photo-to-current ratio can reach 0.12 A W^{-1} and 4.5, respectively, which shows that detectors based on CZGO/ZnO NW heterojunctions have good detectability, and a novel UV PD was designed.

2. Experimental Section

2.1. Growth of Zn-Doped CuGaO_2 Nanoplates

CZGO NPs were synthesized via a facile hydrothermal reaction according to the previous report. For the Zn-doped CGO NP

synthesis, additional $\text{Zn}(\text{NO}_3)_2 \cdot 6\text{H}_2\text{O}$ was added in the reaction to replace part of Ga^{2+} with Zn^{2+} . Briefly, 3.5 mmol $\text{Cu}(\text{NO}_3)_2 \cdot 3\text{H}_2\text{O}$ and $3.5-x$ mmol $\text{Ga}(\text{NO}_3)_3 \cdot 9\text{H}_2\text{O}$ and x mmol $\text{Zn}(\text{NO}_3)_2 \cdot 6\text{H}_2\text{O}$ were dissolved in 35 mL deionized water. Then, 17.5 mmol KOH was dissolved in 17.5 mL deionized water. The deep blue solution was diluted with ethylene glycol and deionized water (the capacity ratio of ethylene glycol and deionized water was 1/3) and transferred into a 100 mL reactor (filled to 70% volume capacity). After reacting at 190°C for 56 h, it was naturally cooled to room temperature. The samples were repeatedly cleaned with ethanol, water, dilute HNO_3 , and ammonia water and finally stored in an ethanol solution. SEM was used to investigate the structure and morphology of CZGO NPs, which can be seen in Figure 1a,b. Zn-doped CGO NPs with a perfect hexagon morphology were synthesized successfully. The diameter of the synthesized CZGO NPs was about 5–6 μm .

The XRD patterns of pure CGO NPs and CZGO NPs are displayed in Figure 1c. All the diffraction peaks could be indexed to JCPDS NO. 41–0255; no other diffraction peaks were discovered in the pattern. Furthermore, the pattern displayed in the inset of Figure 1c is the enlarged XRD 006 diffraction peak and shows a shift to a smaller angle with Zn ion doping. This phenomenon is speculated to be caused by the lattice bending caused by the stress of high-strength Zn or covalent bonds, and results in some lattice deformation. XPS measurements were conducted to evaluate the elemental composition and chemical state of the CZGO NPs shown in Figure 2. The survey spectrum (Figure 2a) indicates the presence of Cu, Ga, and Zn elements. It was sufficient to draw a conclusion that Zn had been doped into the CGO NPs under hydrothermal reaction.

For the heterojunction synthesis, Zn-doped CGO NPs were prepared by the hydrothermal method described in a previous work. According to the previous study, the specific reaction

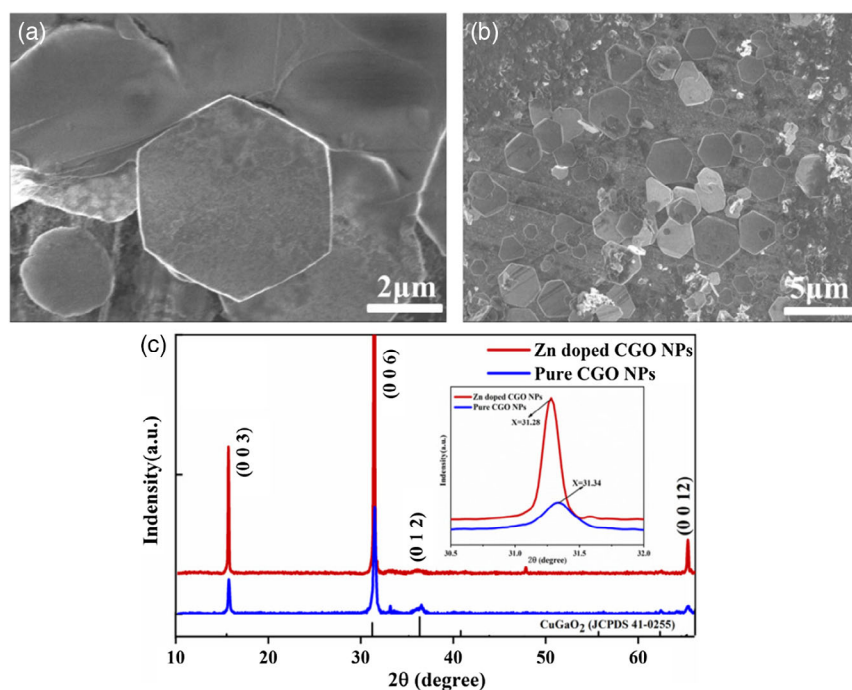


Figure 1. a,b) SEM images of Zn-doped CuGaO_2 NPs and c) XRD spectrum of pure CGO NPs and Zn-doped CGO NPs.

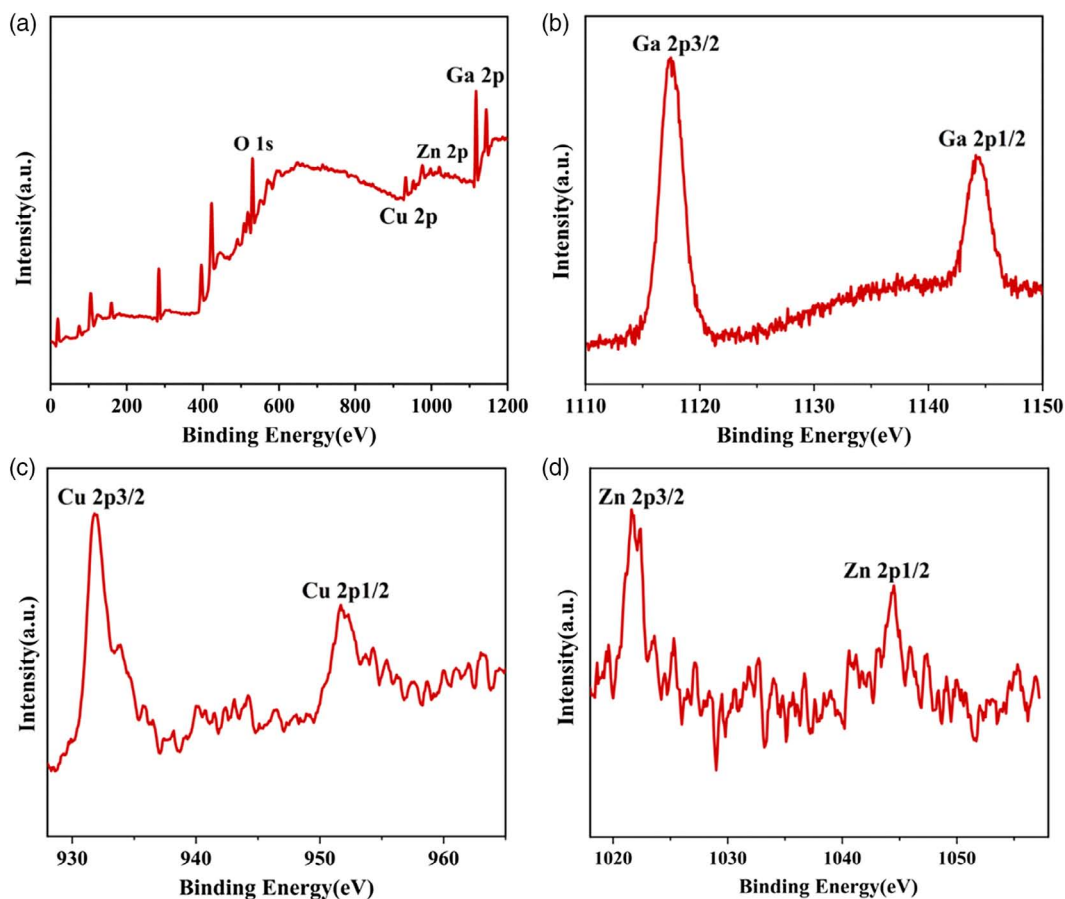
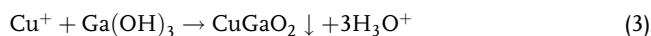


Figure 2. a) XPS survey spectrum of the CZGO NPs, and enlarged view of the b) Ga 2p, c) Cu 2p, and d) Zn 2p peaks.

of CGO phase formation in the hydrothermal reaction is as follows^[39]



2.2. Synthesis of Zn-Doped CGO NP/ZnO NW Heterojunctions

First, the CGO NPs were uniformly dispersed in ethanol by an ultrasonic machine and transferred to a 1 cm × 1.6 cm Si substrate. The substrate was then facedown placed in a hydrothermal reaction frame and immersed in an equimolar (10 mmol) mixed solution of $\text{Zn}(\text{NO}_3)_2 \cdot 6\text{H}_2\text{O}$ and hexamethyltetramine (HMT). The solution was then heated at 90 °C for 4 h to grow heterojunctions. After the reactions, the substrate was cleaned by distilled water and dried in an N_2 atmosphere. As shown in the SEM images in **Figure 3a,b**, numerous CZGO/ZnO heterojunctions were observed, which suggested that ZnO NWs were grown vertically on CGO NPs after the hydrothermal reaction. The successful growth of ZnO NWs was further confirmed by XRD characterization, as shown in **Figure 3c**. There was no difference in

diffraction peaks for the CZGO/ZnO heterojunctions compared with pure CGO NPs. Nevertheless, an emerging diffraction peak corresponding to the (002) plane diffraction for wurtzite ZnO (JCPDS No. 36-1451) could be observed. This result provided evidence that CZGO NP/ZnO NW heterojunctions had been synthesized successfully through a simple hydrothermal method. The sizes of the NWs were almost the same and they were arranged tightly. Therefore, the heterojunctions increased the overall specific surface area.

3. Results and Discussion

3.1. UV Absorption and SEM Image of UV Photodetector

The normalized absorbance spectra of CGO NPs and CZGO NP/ZnO NW heterojunctions are shown in **Figure 4a**. For the CGO NPs and CZGO NP/ZnO NW heterojunctions, the absorption peaks are located at 323 and 337 nm, respectively. The CZGO NP/ZnO NW heterojunctions appear redshifted in the absorption spectrum compared with pure CGO NPs. This phenomenon could be attributed to the sub-bandgap absorption effect, which is caused by the built-in electric field between the p and n junctions.^[40] Furthermore, the energy bandgap E_g can be estimated by the equation^[41]

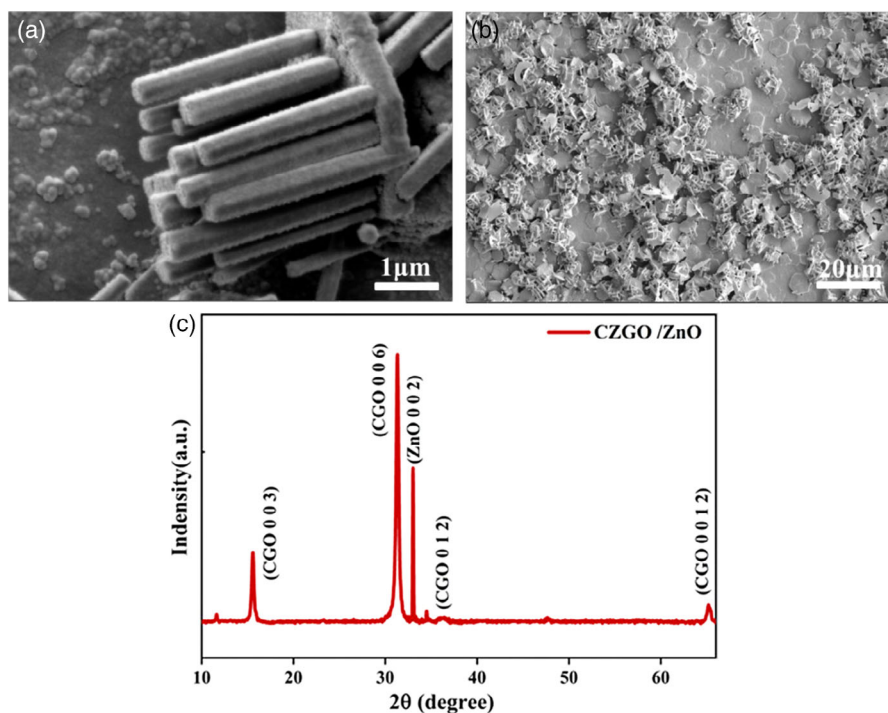


Figure 3. a,b) SEM images of CZGO NP/ZnO NW heterojunctions and c) XRD spectrum of CZGO NP/ZnO NW heterojunctions.

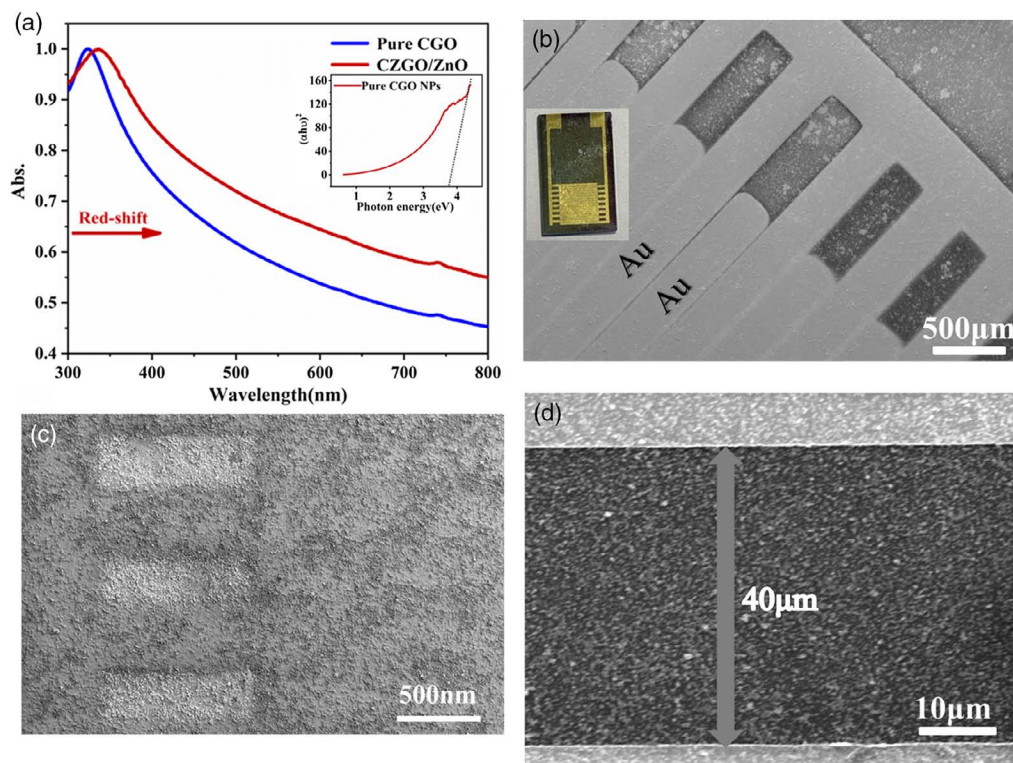


Figure 4. a) UV-vis absorption spectra of the CGO NPs and CZGO/ZnO NW heterojunctions; the inset shows the corresponding plot analysis of the optical bandgap of CGO. SEM images of UV PD based on the b) CGO NPs and c) CZGO/ZnO NW heterojunctions; the inset of (b) shows the physical map of the UV detector. d) SEM image of the electrode space.

$$\alpha E = A(E - E_g^{\text{direct}})^{0.5} + B(E - E_g^{\text{indirect}} \pm E_{\text{phon}})^2 \quad (4)$$

where α is the absorption coefficient, A and B are two fitting parameters, E_g^{indirect} and E_g^{direct} are the indirect and direct gaps, and E_{phon} is the phonon energy. Thus, $(\alpha E)^2$ indicate direct gaps and $(\alpha E)^{0.5}$ indicate indirect gaps. E_g is determined to about 3.7 eV for CGO NPs, as shown in inset of Figure 4a.

p-type silicon was used as a substrate to fabricate the device. The prepared microchips or heterojunctions were spin coated on the Si substrate and dried in nitrogen. Then pairs of Au electrodes were patterned on top of the film by magnetron sputtering. The following Figure 4b,c is the SEM image of the UV detector based on the CGO NPs and CGO/ZnO heterojunctions, respectively. The physical map of the UV detector is shown in inset of Figure 4b. The tight heterojunctions were connected by the electrode space. Figure 4d shows a pair of Au electrodes were separated by a space of 40 μm .

3.2. Optoelectronic Performance

Figure 5a presents the typical I - V curves obtained from the device under dark and illuminated conditions ($\lambda = 365$ nm, 20 mW cm^{-2}). The embedded image is an enlarged I - V

diagram (6 to -10 V). The photocurrent is increased with the applied bias voltage increasing; the highest photocurrent reaches up to 1.18 mA, the dark current is ≈ 0.995 mA, and the photo-to-current ratio (R_s) $(I_{\text{ph}} - I_{\text{dark}})/I_{\text{dark}}$ is estimated to be 0.19. The responsivity value (R) $(I_{\text{ph}} - I_{\text{dark}})/PA$ is $\approx 0.033 \text{ A W}^{-1}$, which is a critical parameter to determine the sensitivity of optoelectronic devices. P is the light power and A represents the effective illuminated area on the detector surface. Response speed and repeatability are key parameters to examine the capability of a PD. Figure 5b shows the on-off state of the detector under light conditions. A cliffy rise and decay can be seen in the enlarged portions of 48.5–50.5 and 58–63 s, which correspond to the on-state and off state, respectively, as shown in Figure 5c,d. The rise time τ_r (from 10% to 90% of the maximum photocurrent) and decay time τ_d (from 90% to 10% of the maximum photocurrent) are estimated to be 0.75 and 0.3 s, respectively, demonstrating a rapid response property especially.

The inset of Figure 6a shows the process of obtaining a photocurrent by UV PDs under illumination. Performance parameters of the UV detectors fabricated from CZGO NP/ZnO NW heterojunctions have been measured. As shown in Figure 6a, I_{ph} is about 0.83 mA and I_{dark} is about 0.15 mA under 10 V

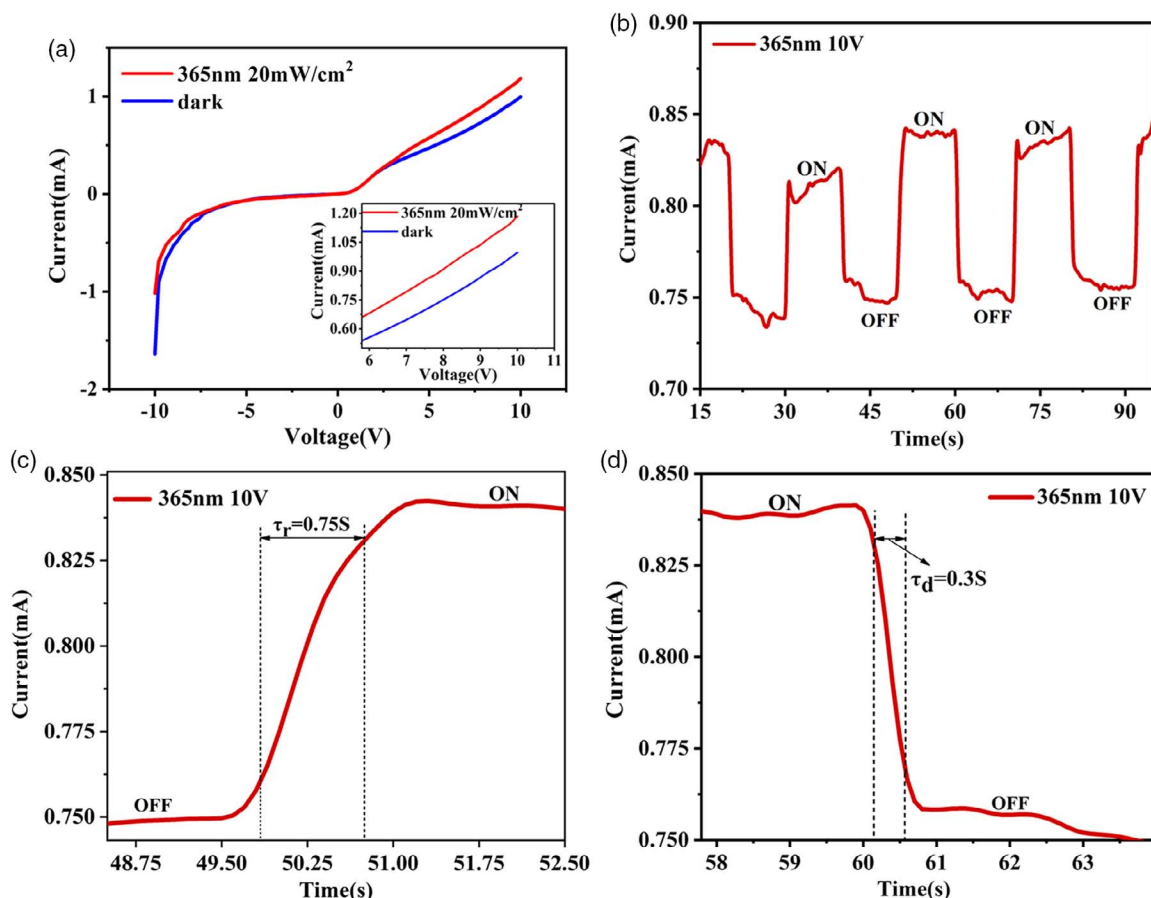


Figure 5. a) Typical I - V curves of the CGO ultraviolet detector illuminated with light of 365 nm and under dark conditions. b) I - T curves during light on-off switching at 10 V under 365 nm illumination. c,d) Enlarged portions in range of 48.5–50.5 and 58–63 s corresponding to light-off to light-on and light-on to light-off transitions.

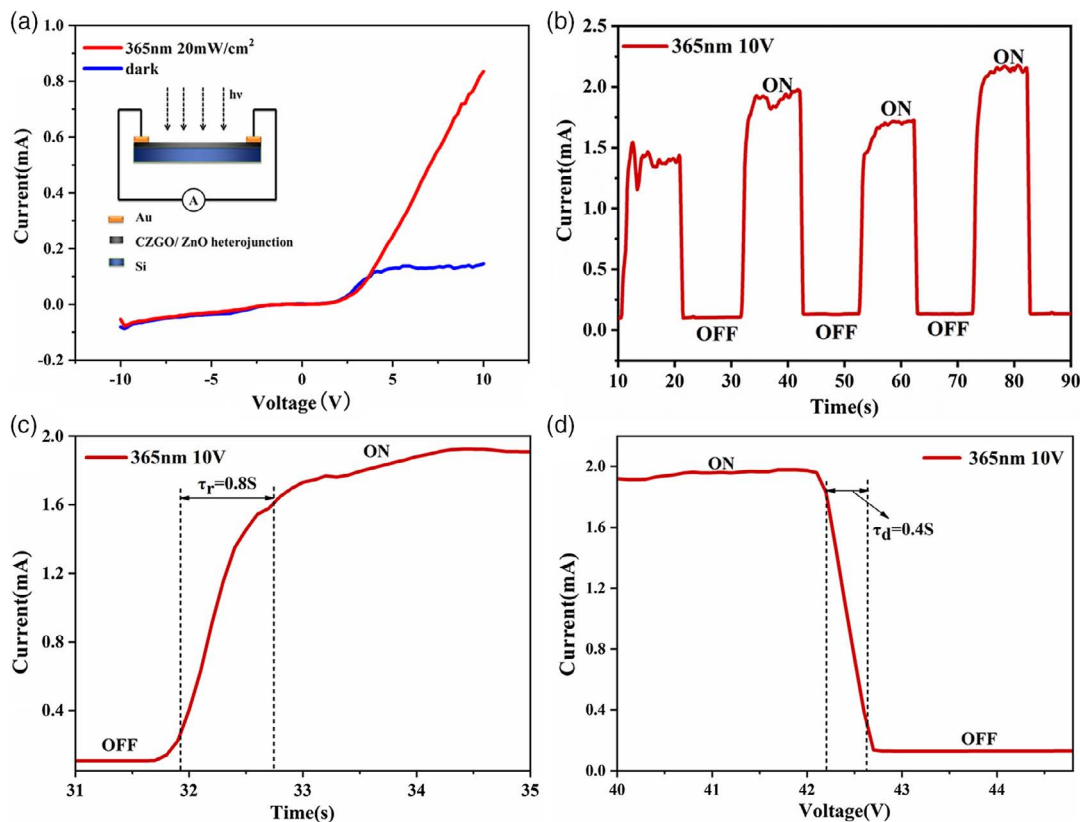


Figure 6. a) Typical I – V curves of the CZGO NP/ZnO NW heterojunction ultraviolet detector illuminated with light of 365 nm and under dark conditions; the inset is the process of obtaining photocurrent by UV PDs under illumination. b) I – T curves during light on–off switching at 10 V under 365 nm illumination. c, d) Enlarged portions in range of 31–35 and 40–45 s corresponding to light-off to light-on and light-on to light-off transitions.

applied bias. Use of a hand-held UV lamp to irradiate the detector surface inevitably makes the light distance and effective light area become variable. Finally, the highest photocurrent value in the time response test is different from that of the I – V test. It is worth noting that the UV detectors based on CZGO NP/ZnO NW heterojunctions have significant photo-current ratio and responsivity values, 4.5 and 0.12 A W^{-1} , respectively. The performance parameters of the detectors fabricated with ZnO NW arrays show that the response value is 0.05 A W^{-1} .^[42] The response value of the heterojunction detector is 2 times that of the ZnO NW array detector and about 4 times that of the CGO NPs. This is a significant result compared with the performance of those of ZnO-based PDs in **Table 1**. Interestingly, the photo-to-current ratio of the heterojunctions is ≈ 23 times that of the CGO NPs. Four repeated cycles under a switching light intensity of 20 mW cm^{-2} are shown in Figure 6b. In the enlarged view, the rise and decay curves of the time-dependent photocurrent response are provided in Figure 6c, d. The rise time τ_r and decay time τ_d were calculated to 0.8 and 0.4 s. Heterojunctions were composed of CZGO NPs and ZnO NWs, which made the heterojunctions have a larger specific surface area than each individual material. The conductivity increased under the illumination condition. Even after turning off the light, the conductivity continued to decrease slowly for a period of time. The photoconductivity

(PPC) effect is the reason for the increase of the τ_r and τ_d . Therefore, analysis of the photoelectric performance parameters of CZGO NP/ZnO NW heterojunctions has great potential to prepare UV PDs.

We speculate that CZGO NP/ZnO NW heterojunctions can improve detection performance for the following reasons: 1) nanostructures can improve the energy conversion efficiency remarkably via various light-trapping mechanisms.^[43] Due to the particularly large intrinsic gain and long interaction length, vertical ZnO NW arrays can capture most incident UV light and generate a strong light-trapping effect.^[44] Meanwhile, ZnO NWs were grown vertically and tightly on CZGO NPs, which promotes increase of the specific surface area and enhances the ability to capture photons. 2) The synergistic effect of p-type CZGO and n-type ZnO promotes faster separation of electrons and holes. The heterojunctions form a depletion region at the CZGO NP and ZnO NW interface through carrier diffusion, forming a built-in electric field at the interface. Driven by this built-in electric field inside the depletion region, holes in CZGO and electrons in ZnO can be easily separated at a faster rate. Furthermore, as the intercrystalline contacts increase and the electron transportation path extends in the vertical direction, faster electron–hole recombination occurs in the vertical orientation rod geometry; this could be the reason that heterojunctions make the photocurrent reduce slightly.^[45,46]

Table 1. Comparison of the characteristic parameters of different PDs.

Photodetectors	λ [nm]	Bias [V]	Photo-to-current ratio $R_s = (I_{ph} - I_{dark})/I_{dark}$	Responsivity value $(I_{ph} - I_{dark})/PA [A W^{-1}]$	τ_r [s]	τ_d [s]	Ref.
ZnO nanorod array	365	1	5.13×10^2	–	–	1.69	[47]
ZnO films	365	3	17.03	0.00044	4.172	11.012	[48]
ZnO nanorods	370	3	–	0.198	0.993	2.036	[49]
Craphene/ZnO	365	–5	–	23	3	0.5	[50]
ZnO NWs	360	1	11.25	≈ 0.39	2	100	[51]
CGO NPs	365	10	0.19	0.033	0.7	0.3	This work
CZGO/ZnO	365	10	4.5	0.12	0.8	0.4	This work

4. Conclusions

In summary, this study reports the optoelectronic properties of UV PDs based on pure CGO NPs and CZGO NP/ZnO NW heterojunctions. The CZGO NP/ZnO NW heterojunctions have better optoelectronic performance parameters than pure CGO NPs. The results express that the response value of the heterojunctions detector is ≈ 4 times that of the CGO NPs. Interestingly, the photo-to-current ratio of the heterojunctions is ≈ 23 times that of the CGO NPs. Due to the high lattice matching, hexagonal wurtzite ZnO NWs are grown vertically on the surface of CZGO NPs. Therefore, the heterojunctions increase the overall specific surface area and enhance the photon capture ability. This work mainly focuses on the synergistic effect of p-type CGO NPs with n-type nanostructures, which provides a new idea for the rational design of optoelectronic devices.

Acknowledgements

This work was financially supported by the National Natural Science Foundation of China (Nos. 61804014, 61805023, and 61804013); The Excellent Youth Foundation of Jilin Province (No. 20180520194JH); Changchun University of Science and Technology Youth Science Foundation (No. XQNJJ-2017-20); Jilin Science and Technology Development Plan (Grant No. 20180519018JH); and The Research Foundation of Jilin province (Grant No. 20180519004JH).

Conflict of Interest

The authors declare no conflict of interest.

Keywords

CuGa_{1-x}Zn_xO₂ nanoplates, heterojunctions, ultraviolet photodetectors

Received: October 31, 2019

Revised: December 18, 2019

Published online: January 14, 2020

[1] A. Novack, M. Gould, Y. Yang, Z. Xuan, M. Streshinsky, Y. Liu, G. Capellini, A. E. J. Lim, G. Q. Lo, T. B. Jones, M. Hochberg, *Opt. Express* **2013**, 21, 28387.

- [2] X. S. Luo, J. F. Song, X. G. Tu, Q. Fang, L. X. Jia, Y. Huang, T. Y. Liow, M. B. Yu, G. Q. Lo, *Opt. Express* **2014**, 22, 20020.
- [3] C. Xie, X. Lu, X. Tong, Z. Zhang, F. Liang, L. Liang, *Adv. Funct. Mater.* **2019**, 29, 1806006.
- [4] H. Lu, W. Tian, F. Cao, Y. Ma, B. Gu, L. Li, *Adv. Funct. Mater.* **2016**, 26, 1296.
- [5] D. S. Tsai, K. K. Liu, D. H. Lien, M. L. Tsai, C. F. Kang, C. A. Lin, L. J. Li, J. H. He, *ACS Nano* **2013**, 7, 3905.
- [6] S. M. Hatch, J. Briscoe, S. Dunn, *Adv. Mater.* **2013**, 25, 867.
- [7] Z. Yang, M. Q. Wang, J. J. Ding, Z. W. Sun, L. Li, J. Huang, J. Liu, J. Y. Shao, *ACS Appl. Mater. Interfaces* **2015**, 7, 21235.
- [8] K. Roy, M. Padmanabhan, S. Goswami, T. P. Sai, G. Ramalingam, S. Raghavan, A. Ghosh, *Nat. Nanotechnol.* **2013**, 8, 826.
- [9] H. Chen, P. Verheyen, P. De Heyn, G. Lepage, J. De Coster, S. Balakrishnan, P. Absil, W. Yao, L. Shen, G. Roelkens, J. Van Campenhout, *Opt. Express* **2016**, 24, 4622.
- [10] L. Viro, D. Benedikovic, B. Szlag, C. Alonso-Ramos, B. Karakus, J. M. Hartmann, X. L. Roux, P. Crozat, E. Cassan, D. Marris-Morini, C. Baudot, F. Boeuf, J. M. Fédeli, C. Kopp, L. Vivien, *Opt. Express* **2017**, 25, 19487.
- [11] Y. Sun, K. Zhou, Q. Sun, J. P. Liu, M. X. Feng, Z. C. Li, Y. Zhou, L. Q. Zhang, D. Y. Li, S. M. Zhang, M. S. Lkeda, S. Liu, H. Yang, *Nat. Photonics* **2016**, 10, 595.
- [12] W. Kong, G. Wu, K. Wang, T. Zhang, Y. Zou, D. Wang, L. Luo, *Adv. Mater.* **2016**, 28, 10725.
- [13] N. Aggarwal, S. Krishna, A. Sharma, L. Goswami, D. Kumar, S. Husale, G. Gupta, *Adv. Electron. Mater.* **2017**, 3, 1.
- [14] H. Shen, C. X. Shan, B. H. Li, B. Xuan, D. Z. Shen, *Appl. Phys. Lett.* **2013**, 103, 232112.
- [15] Y. Z. Jin, J. P. Wang, B. Q. Sun, J. C. Blakesley, N. C. Greenham, *Nano Lett.* **2008**, 8, 1649.
- [16] G. Liu, N. Hoivik, X. Wang, S. Lu, K. Wang, H. Jakobsen, *Electrochim. Acta* **2013**, 93, 80.
- [17] X. Fang, J. Yan, L. Hu, H. Liu, P. S. Lee, *Adv. Funct. Mater.* **2012**, 22, 1613.
- [18] H. Liu, L. F. Hu, K. Watanabe, X. H. Hu, B. J. Dierre, B. Kim, T. Sekiguchi, X. S. Fang, *Adv. Funct. Mater.* **2013**, 23, 3701.
- [19] Y. Tsao, S. Chowdhury, M. A. Hollis, D. Jena, N. M. Johnson, K. A. Jones, R. J. Kaplar, S. Rajan, C. G. Van de Walle, E. Bellotti, C. L. Chua, R. Collazo, M. E. Coltrin, J. A. Cooper, K. R. Evans, S. Graham, T. A. Grotjohn, E. R. Heller, M. Higashiwaki, M. S. Islam, P. W. Juodawilkis, M. A. Khan, A. D. Koehler, J. H. Leach, U. K. Mishra, R. J. Nemanich, R. C. N. Pilawa-Podgurski, J. B. Shealy, Z. Sitar, M. J. Tadjer, et al., *Adv. Electron. Mater.* **2018**, 4, 1600501.
- [20] L. Peng, L. Hu, X. Fang, *Adv. Mater.* **2013**, 25, 5321.
- [21] L. Peng, L. F. Hu, X. S. Fang, *Adv. Mater.* **2013**, 25, 5321.

- [22] J. M. Goodman, J. Aarons, *Proc. IEEE* **1990**, *78*, 512.
- [23] A. N. Banerjee, K. K. Chattopadhyay, *Prog. Cryst. Growth Charact. Mater.* **2005**, *50*, 52.
- [24] L. J. Mandalapu, F. X. Xiu, Z. Yang, D. T. Zhao, J. L. Liu, *Appl. Phys. Lett.* **2006**, *88*, 92103.
- [25] M. J. Han, K. Jiang, J. Z. Zhang, Y. W. Li, Z. G. Hu, J. H. Chu, *Appl. Phys. Lett.* **2011**, *99*, 2011.
- [26] A. Renaud, B. Chavillon, L. L. Pleux, Y. Pellegrin, E. Blart, M. Boujtita, T. Pauporté, L. Cario, S. Jobic, F. Odobel, *J. Mater. Chem.* **2012**, *22*, 14353.
- [27] S. B. Bashar, C. X. Wu, M. Suja, H. Tian, W. H. Shi, J. L. Liu, *Adv. Opt. Mater.* **2016**, *4*, 2063.
- [28] X. B. Tang, G. M. Li, S. M. Zhou, *Nano. Lett.* **2013**, *13*, 5046.
- [29] B. B. Lv, Y. W. Tang, S. Y. Lou, Y. L. Xu, S. M. Zhou, *J. Mater. Chem. C* **2016**, *4*, 5416.
- [30] Ü. Özgür, Y. I. Alivov, C. Liu, A. Teke, M. A. Reshchikov, S. Doğan, V. Avrutin, S.-J. Cho, H. Morkoç, *J. Appl. Phys.* **2005**, *98*, 41301.
- [31] C. Chen, S. Zhang, B. Hu, H. San, Z. Cheng, W. Hofmann, *Composites B, Eng.* **2019**, *164*, 640.
- [32] L. X. Zheng, F. Teng, Z. M. Zhang, B. Zhao, X. S. Fang, *J. Mater. Chem. C* **2016**, *4*, 10032.
- [33] Z. Xu, D. H. Xiong, H. Wang, W. J. Zhang, X. W. Zeng, L. Q. Ming, W. Chen, X. B. Xu, J. Cui, M. K. Wsang, S. Powar, U. Bach, Y. B. Cheng, *Mater. Chem. A* **2014**, *2*, 2968.
- [34] H. Chen, K. Liu, L. Hu, A. A. Al-Ghamdi, X. Fang, *Mater. Today* **2015**, *18*, 493.
- [35] L. Peng, L. Hu, X. Fang, *Adv. Funct. Mater.* **2014**, *24*, 2591.
- [36] H. Y. Chen, C. C. Yang, *Surf. Coatings Technol.* **2013**, *231*, 277.
- [37] R. Shannon, *Acta Crystallogr. A* **1976**, *32*, 751.
- [38] C. Y. Tsay, C. L. Chen, *Ceram. Int.* **2017**, *11*, 2563.
- [39] Y. M. Li, Y. Song, Y. C. Jiang, M. X. Hu, Z. C. Pan, X. J. Xu, H. Y. Chen, Y. S. Li, L. F. Hu, X. S. Fang, *Adv. Funct. Mater.* **2017**, *27*, 1701066.
- [40] P. Q. Li, H. T. Hu, J. F. Xu, H. Jing, H. Peng, L. Jing, C. X. Wu, S. Y. Ai, *Appl. Catal. B, Environ.* **2014**, *147*, 912.
- [41] M. Meinert, G. Reiss, *J. Phys. Condens. Matter.* **2014**, *26*, 115503.
- [42] L. Liu, W. Yang, W. Sun, Q. Li, J. K. Shang, *ACS Appl. Mater. Interfaces* **2015**, *7*, 1465.
- [43] B. Nie, J. Hu, L. Luo, C. Xie, L. Zeng, P. Lv, F. Li, *Small.* **2013**, *17*, 2872.
- [44] S. Leung, Q. Zhang, F. Xiu, D. Yu, J. C. Ho, D. Li, Z. Fan, *J. Phys. Chem. Lett.* **2014**, *5*, 1479.
- [45] L. Li, X. S. Fang, T. Zhai, M. Liao, U. K. Gautam, X. Wu, Y. Koide, Y. Bando, D. Golberg, *Adv. Mater.* **2010**, *22*, 4151.
- [46] L. B. Wang, W. Y. Yang, H. N. Chong, L. Wang, F. M. Gao, L. H. Tian, Z. B. Yang, *RSC Adv.* **2015**, *5*, 52388.
- [47] F. Yi, Q. Liao, X. Yan, Z. Bai, Z. Wang, X. Chen, Q. Zhang, Y. Huang, Y. Zhang, *Physica E: Low-Dimens. Syst. Nanostruct.* **2014**, *61*, 180.
- [48] P. Gu, X. Zhu, D. Yang, *Appl. Phys. A, Mater. Sci. Process.* **2019**, *125*, 50.
- [49] P. Gu, X. Zhu, D. Yang, *J. Alloys Compd.* **2020**, *815*, 152346.
- [50] B. D. Boruah, A. Mukherjee, A. Misra, *Nanotechnology* **2016**, *27*, 95205.
- [51] W. Y. Weng, S. J. Chang, C. L. Hsu, T. J. Hsueh, S. P. Chang, *J. Electrochem. Soc.* **2010**, *157*, 30.